# Phase-factor-optimized topological transmission in a dimerized lattice with long-range hopping

Li-Na Zheng,[1] Xiu-Yun Zhang,[2] Ai-Lei He,[2] and Lu Qi[2,*]

[1]*Center for Quantum Sciences and School of Physics, Northeast Normal University, Changchun, Jilin 130024, China*

[2]*School of Physical Science and Technology, Yangzhou University, Yangzhou 225002, China*

(Received 15 April 2024; accepted 12 July 2024; published 1 August 2024)

We show that both the efficiency and robustness of the topological excitation transmission can be optimized by the phase factor of the long-range hopping in the dimerized lattice. This phenomenon can be explained as the fact that the phase factor in the hopping can widen the minimal energy space around the gap closing point. By redesigning the configuration of long-range hopping, we implement the perfect topological excitation transmission assisted by the phase factor from the left edge to the right edge. We demonstrate that the present optimized topological excitation transmission essentially originates from the phase transition induced by the phase factor, in which the existence of the phase transition leads to the decreasing of the gap closing points. Furthermore, we also investigate the generalized cases with longer-range hopping and find that the optimized topological excitation transmission is determined by the order of long-range hopping. Our investigation shows the significant effect of the phase factor of hopping strength on the topological excitation transmission, which is usually overlooked in relevant work.

DOI: 10.1103/PhysRevA.110.022401

## I. INTRODUCTION

Topological pumping [1–25], that is, implementing excitation transmission by a topological insulator [26–29], has recently been drawing increasing attention. Based on the global protection of the topology, the topological pumping can resist certain local disorder, providing potential applications in quantum information processing [12]. Two typical examples of topological pumping are quantized bulk transmission and nonquantized edge transmission. The former, specifically, Thouless pumping [1], reveals the intrinsic connection between the transport property and topological invariant, while the latter can realize the robust excitation transmission between two remote nodes along the boundary, for example, the robust topological edge transmissions in quasicrystals [9], dipolar arrays [11], linear networks [12], and superconducting circuit lattices [15]. The topological transmissions along the boundary state usually need to satisfy the adiabatic condition to avoid the evolution entering the bulk around the gap closing point. Thus, accelerated topological transmission schemes are implemented based on Landau-Zener tunneling [17], adiabatic passage [18], long-range hopping [20], and coupling engineering [22,24,25].

We note that the phase factor in the hopping strength shows unique effects on topological properties [30–36]. One of the most well-known examples is the Haldane model [30], in which the phase factor originating from staggered magnetic flux in the hopping can induce the topological phase transition. In addition to inducing the phase transition, the phase factor can also induce a topological flat band [37–42] and high-order topological state [43,43–49]. For example, a series of topological flat bands with higher Chern numbers has been shown by introducing the distant-neighbor hopping terms with staggered magnetic fluxes into the monolayer star lattice [42]. Furthermore, in Ref. [49] some of the present authors showed that the Chern insulator and higher-order topological insulator states can appear by considering the nearest-neighbor (NN) hopping with a suitable phase factor and the next-nearest-neighbor hopping terms simultaneously. We note that, although the relevant explorations of the phase factor in hopping on topological properties have been widely investigated, whether the topology affected by the phase factor can change the topological excitation transmission seems to be an open problem. In particular, current topological transmission schemes are mostly focused on the design of the hopping amplitude; thus the exploration of the direct impact of the phase factor on topological transmission will be an interesting topic.

In this paper we investigate the effects of the phase factor in long-range hopping on the topological excitation transmission and find that the phase factor can enhance the efficiency and robustness of the transmission in certain cases. We reveal that the enhanced transmission originates from the widened minimal energy space around the gap closing point, in which the widened gap space can relax the restrictions of the adiabatic condition. Together with optimizing the configuration of long-range hopping, we show the perfect topological excitation transmission enhanced by the phase factor. We demonstrate that, by the phase diagram, the transmission enhanced by the phase factor is essentially induced by the phase transition caused by the phase factor, in which the phase transition can decrease the number of gap closing points. We also investigate the effects of the phase factor in longer-range hopping on the topological excitation transmission and we find that the order of the long-range hopping can affect the effects of the phase factor. Our investigation reveals the potential connections among the phase factor, phase transition, and topological excitation transmission, which can provide different views on the effects of the phase factor.

*Contact author: luqi@yzu.edu.cn

 

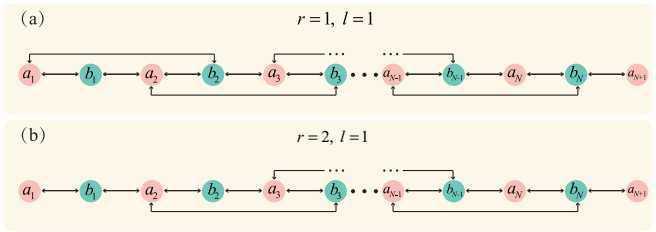


FIG. 1. Schematic diagram of the dimerized lattice chain with long-range hopping when (a) $r=1$ and $l=1$ and (b) $r=2$ and $l=1$.

The paper is organized as follows. In Sec. II we show the phase-factor-enhanced topological excitation transmission and reveal the intrinsic physical mechanisms. A summary is given in Sec. III.

## II. TOPOLOGICAL TRANSMISSION ENHANCED BY THE PHASE FACTOR IN LONG-RANGE HOPPING

### A. Model and Hamiltonian

We consider a dimerized lattice chain with long-range hopping, which can be described by the Hamiltonian

$$H = \sum_n (J_1 a_n^\dagger b_n + J_2 a_{n+1}^\dagger b_n + \text{H.c.}) + \sum_{n=r} (J a_n^\dagger b_{n+l} + J^* b_{n+l}^\dagger a_n). \quad (1)$$

Here $J_j = 1 + (-1)^j \cos\theta$ ($j = 1, 2$ and $\theta \in [0, 2\pi]$) is the real NN hopping, $J = |J|e^{i\gamma}$ (amplitude $|J|$ and phase factor $\gamma$) is the complex long-range hopping between sites $a_n$ and $b_{n+l}$, $l$ is the length between two unit cells, and $r$ represents the initial location of adding the long-range hopping. Figure 1 shows two different lattice structures for different $r$ and $l$, specifically, $r = l = 1$ in Fig. 1(a) and $r = l + 1 = 2$ in Fig. 1(b). When the amplitude of long-range hopping satisfies $|J| = 0$, the present lattice becomes a standard Su-Schrieffer-Heeger (SSH) chain, in which the odd-sized SSH chain has a zero-energy mode, as shown in Fig. 2(a). The special localization properties of the zero-energy mode [Fig. 2(b)] are widely used to implement the topological excitation transmission [15], i.e., the excitation initially prepared at the left edge with $|L\rangle = |1, 0, 0, \ldots, 0, 0, 0\rangle$ can be transmitted to the right edge via the Schrödinger equation $i\frac{\partial}{\partial t}|L\rangle = H(\theta_t)|L\rangle$. Here $\theta_t = \Omega t$ is the time-dependent version of the parameter $\theta$, with $\Omega$ the varying rate and $t$ time.

Usually, one of the main themes in topological excitation transmission is how to realize the fast and efficient excitation exchange using the topological channel. According to the adiabatic theory, the minimal energy space between the gap and bulk states [$\Delta_E$ in Fig. 2(a)] determines the speed of transmission, i.e., $\sqrt{\Omega} < \Delta_E$ [15], which suggests that we can implement the efficient topological excitation transmission by designing a larger energy space $\Delta_E$. The minimal energy space $\Delta_E$, when $r = 1$ and $l = 1$, versus the amplitude and phase factor of the long-range hopping is shown in Fig. 2(c). Obviously, when $\gamma = 0$, the minimal energy space $\Delta_E$ decreases with increasing amplitude $|J|$. In contrast, the minimal energy space $\Delta_E$ can be enlarged for a certain value of $|J|$ when $\gamma \neq 0$, e.g., the system has a maximal $\Delta_E$ when $|J| = 1.328$ and $\gamma = -\pi$. The energy spectrum for the maximal $\Delta_E$ is shown in Fig. 2(d), in which the minimal energy space $\Delta_E$ indeed becomes much larger than in Fig. 2(a).

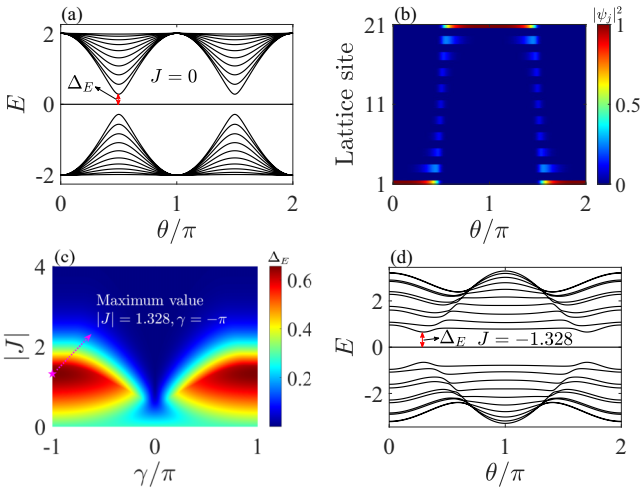


FIG. 2. Energy spectra, distribution of state, and minimal energy space. (a) Energy spectrum versus periodic parameter $\theta$ when $J = 0$. The minimal energy space around the gap closing point is denoted by $\Delta_E$. (b) Distribution of the zero-energy mode in (a). (c) Minimal energy space $\Delta_E$ versus phase factor $\gamma$ and amplitude $|J|$ in long-range hopping. (d) Energy spectrum versus periodic parameter $\theta$ when $J = -1.328$. The size of the lattice is set as $L = 21$.

### B. Phase-factor-accelerated topological excitation transmission

The enlarged energy space $\Delta_E$ may lead to accelerated topological excitation transmission. To estimate the effects of the amplitude $|J|$ and phase factor $\gamma$ of long-range hopping on the topological excitation transmission, we can define the transmission fidelity $F = |\langle R|\Psi_f\rangle|$. Here $|R\rangle = |0, 0, 0, \ldots, 0, 0, 1\rangle$ is the ideal right edge state and $|\Psi_f\rangle$ denotes the evolved final state obtained from the Schrödinger equation $i\frac{\partial}{\partial t}|L\rangle = H(\theta_t)|L\rangle$. In this way, if the excitation initially prepared at the left edge is transmitted to the right edge successfully, we have $F = 1$. The fidelity versus the amplitude of long-range hopping $|J|$ and varying rate $\Omega$ is shown in Fig. 3(a). We find that, for a given evolution speed $\Omega$, the increased hopping amplitude $|J|$ can suppress the topological excitation transmission, e.g., when $|J| > 1$, the transmission cannot be implemented even if the evolution speed satisfies $\Omega = 10^{-4}$. Significantly, we find that the phase factor of the long-range hopping can promote topological excitation even when $|J| \neq 0$. The fidelity versus the phase factor $\gamma$ and evolution speed $\Omega$ when $|J| = 1$ is shown in Fig. 3(b). The results clearly reveal that the nonvanishing phase $\gamma$ can promote the topological excitation. Specific examples of topological excitation transmission when $\gamma = \pi$ and $\gamma = 0$ are plotted in Figs. 3(c) and 3(d). Obviously, the excitation can be transmitted to the right edge with high fidelity when $\gamma \neq 0$. Note that, when $\gamma \neq 0$, the transmission probability of excitation to the right edge cannot reach $F \sim 1$, i.e., the present topological transmission assisted by phase $\gamma$ corresponds to an imperfect topological transmission.

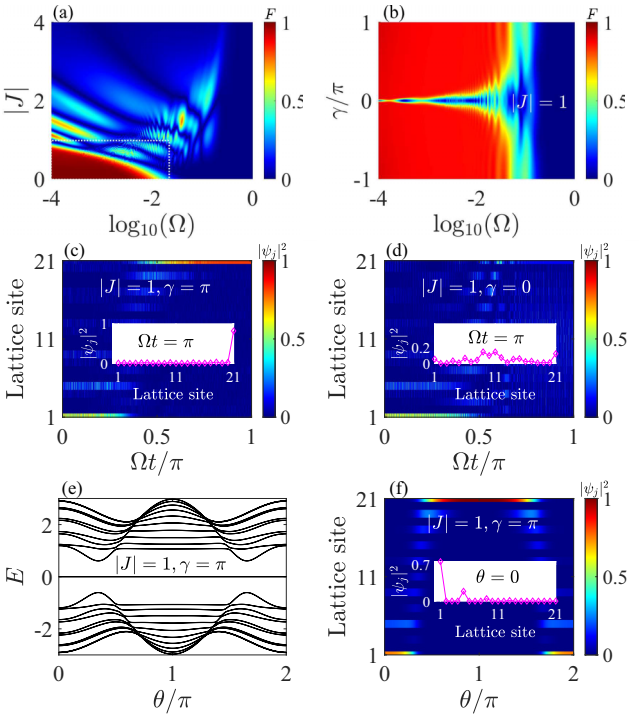


FIG. 3. Fidelity, evolutions of excitation, energy spectrum, and distribution of state when $r=1$ and $l=1$. (a) Fidelity $F$ versus evolution speed $\Omega$ and amplitude of long-range hopping $|J|$ when $\gamma=0$. (b) Fidelity $F$ versus evolution speed $\Omega$ and phase factor of long-range hopping $\gamma$ when $|J|=1$. Evolutions of excitation for (c) $\gamma=\pi$ and (d) $\gamma=0$ when $|J|=1$ and $\Omega=10^{-4}$. The insets show the distributions of excitation at the final time. (e) Energy spectrum versus the parameter $\theta$ when $|J|=1$ and $\gamma=\pi$. (f) Distribution of the zero-energy mode in (a). The inset shows the zero-energy mode now cannot be localized at the left edge completely when $\theta=0$. The lattice size is $L=21$.

The reason originates from the effects of large long-range hopping on the left edge state. The long-range hopping in the present lattice model cannot destroy the chiral symmetry, i.e., the present odd-sized lattice still has a zero-energy mode in the gap. According to the eigenequation of energy, under the basis of lattice sites, the zero-energy mode satisfies

$$\begin{aligned}\psi_{a_2} &= -J_1/J_2\psi_{a_1},\\ \psi_{a_3} &= -J_1/J_2\psi_{a_2} - J/J_2\psi_{a_1},\\ \psi_{a_4} &= -J_1/J_2\psi_{a_3} - J/J_2\psi_{a_2},\\ &\vdots\end{aligned} \tag{2}$$

and

$$\begin{aligned}\psi_{b_2} &= -J_1/J\psi_{b_1},\\ \psi_{b_3} &= -J_1/J\psi_{b_2} - J_2/J\psi_{b_1},\\ \psi_{b_4} &= -J_1/J\psi_{a_3} - J_2/J\psi_{a_2},\\ &\vdots\\ \psi_{b_N} &= -J_1/J_2\psi_{b_{N-1}},\\ J_2\psi_{b_N} &= 0.\end{aligned} \tag{3}$$

Here $\psi_{a_n}$ ($\psi_{b_n}$) denotes the probability amplitude of the zero-energy mode at site $a_n$ ($b_n$). Obviously, we have $\psi_{b_n}=0$ for $n\in[1,N]$, i.e., the zero-energy mode only occupies the $a$-type sites. If we have $|J_1|\ll|J_2|$ (e.g., $\theta\sim 0$) and $\psi_{a_1}=1$, we find that the zero-energy mode is localized at site $a_1$ when $|J|=0$. In contrast, the zero-energy mode can also occupy the site $a_3$ now ($-J/J_2$ tends to a finite value) if the amplitude of long-range hopping is large enough. In this way, the probability amplitude of the zero-energy mode at site $a_1$ will be decreased after the normalization. Thus, the initial state $|L\rangle=|1,0,0,\ldots,0,0,0\rangle$ cannot match the zero-energy mode precisely, leading to the excitation not being able to be transmitted to the right edge completely. For further verification, the energy spectrum and distribution of the zero-energy mode are shown in Figs. 3(e) and 3(f). The distribution of the zero-energy mode clearly shows the nonzero distribution at site $a_3$ when $\theta=0$. Actually, this phenomenon can also be comprehended from the lattice structure. As shown in Fig. 1(a), the long-range hopping has a larger effect on the left edge state due to the existence of the long-range hopping between sites $a_1$ and $b_2$.

To implement the perfect topological excitation transmission assisted by phase $\gamma$, we now consider removing the hopping between sites $a_1$ and $b_2$ [see Fig. 1(b)]. After that, the probability amplitude of the zero-energy mode at site $a_3$ now becomes $a_3=-J_1/J_2a_2$, i.e., the zero energy mode is still mainly localized at the left edge site when $\theta\sim 0$. In Figs. 4(a) and 4(b) we plot the energy spectrum and distribution of the zero-energy mode when $r=2$ and $l=1$ [model in Fig. 1(b)]. Obviously, the zero-energy mode can be localized at the left edge site completely when $\theta=0$, meaning that we may implement the perfect topological excitation transmission assisted by the phase $\gamma$. The minimal energy space $\Delta_E$ versus the hopping amplitude $|J|$ and phase $\gamma$ when $r=2$ and $l=1$ is plotted in Fig. 4(c). We find that, in this case, the phase $\gamma$ can still extend the energy space $\Delta_E$ for a certain finite hopping amplitude $|J|$. For example, as shown in Figs. 4(d) and 4(e), the system has a maximal value of $\Delta_E$, which implies the possible accelerated transmission. To further estimate the transmission efficiency when $r=2$ and $l=1$, the fidelity versus the hopping amplitude and evolution speed is shown in Fig. 4(f). The pattern shows a conclusion similar to the case in Fig. 3(a), i.e., the topological excitation transmission can be implemented when $|J|<1$ and the increased hopping amplitude $|J|$ can tighten the adiabatic condition. In contrast, when we consider the phase $\gamma$, the unsuccessful topological transmission now can be implemented with $F\sim 1$ and the evolution speed can be increased [Fig. 4(g)]. The specific transmission processes when $\gamma=-0.5\pi$ and $\gamma=0$ are shown in Figs. 4(h) and 4(i), which further verify the above conclusions.

### C. Robustness and analysis

In addition to promoting the efficiency of topological excitation transmission, the phase factor $\gamma$ also can enhance the robustness of the transmission process. This is a natural inference since the phase factor $\gamma$ can extend the minimal energy space $\Delta_E$ for a given amplitude of long-range hopping. To verify the above inference, we can calculate the

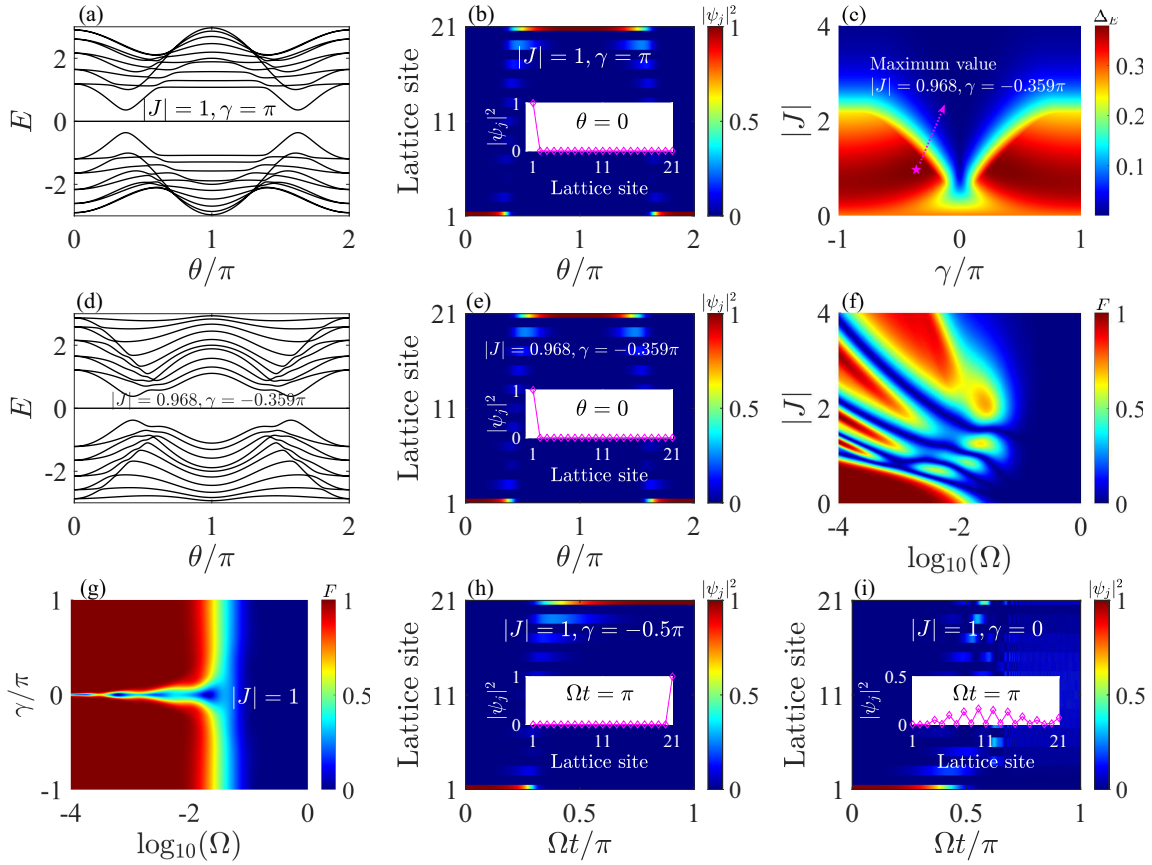


FIG. 4. Topological and transmission properties when $r=2$ and $l=1$. (a) Energy spectrum and (b) distribution of the zero-energy mode when $|J|=1$, $\gamma=\pi$, $r=2$, and $l=1$. (c) Minimal energy space $\Delta_E$ versus the parameters $\gamma$ and $|J|$. (d) Energy spectrum and (e) distribution of the zero-energy mode when $|J|=0.968$ and $\gamma=-0.359\pi$. The inset in (d) shows the complete localization of the zero-energy mode when $\theta=0$. (f) Fidelity versus the evolution speed $\Omega$ and hopping amplitude $|J|$. (g) Fidelity versus the evolution speed $\Omega$ and hopping phase $\gamma$. (h) Perfect topological excitation transmission when $|J|=1$, $\gamma=-0.5\pi$, $r=2$, and $l=1$. (i) Invalid topological transmission when $|J|=1$, $\gamma=0$, $r=2$, and $l=1$. The lattice size is $L=21$.

average fidelity $\bar{F}=\frac{1}{N}\sum F_i$ after considering the massive disorder samples, e.g., $N=100$. Here $F_i=|\langle R|\Psi_{f,i}\rangle|$ represents the fidelity when the disorder in NN hopping $H_{\rm d}=W\sum[(\delta_{a_n}a_n^\dagger b_n+\delta_{b_n}a_{n+1}^\dagger b_n)+\text{H.c.}]$ ($W$ is the disorder amplitude and $\delta_{k_n}\in[-0.5,0.5]$, with $k=a,b$, is a small random quantity) is introduced into the system one time. The average fidelity versus the disorder amplitude $W$ and parameter $|J|$ when the evolution speed satisfies $\Omega=10^{-3}$ is shown in Fig. 5(a). The results indicate that the topological transmission can resist large disorder only when $|J|<0.5$, and the increased parameter $|J|$ can decrease the robustness of transmission. However, the phase factor $\gamma$ can enhance the robustness of topological transmission, as shown in Fig. 5(b). For example, when $\gamma=-\pi$, we find that the topological transmission can be realized even when $W=0.5$ and $|J|=2$.

In the following, we briefly discuss why the phase factor $\gamma$ can enhance the efficiency and robustness of the topological excitation transmission. Note that the transmission efficiency and robustness actually depend on the minimal energy space $\Delta_E$ at the gap closing point for the finite lattice. Thus, the phase transition related to the gap closing point may be the essential regime to enhance the efficiency and robustness of topological excitation transmission. For the case of $r=2$ and $l=1$ in long-range hopping, the translational symmetry is broken, leading to the phase transition being able to be estimated by the winding number defined in real space [50–53], i.e.,

$$\nu=\mathcal{T}\{Q_{\rm BA}[X,Q_{\rm AB}]\}. \tag{4}$$

Here $Q_{\rm BA}=C_{\rm B}QC_{\rm A}$ ($Q_{\rm AB}=C_{\rm A}QC_{\rm B}$), $C_{\rm B}$ ($C_{\rm A}$) is the projection to sublattice $b$ ($a$), $Q=P_+-P_-$ is the matrix defined by the projection operators $P_\pm$ of the positive and negative bands, $X$ is the position operator, and $\mathcal{T}$ denotes the trace per volume.

The phase diagram versus the hopping amplitude $|J|$ and parameter $\theta$ is shown in Fig. 5(c). The results indicate that the increased hopping amplitude $|J|$ can induce a new topological phase with $\nu=-1$, e.g., when $|J|=1$, the system experiences a phase transition between $\nu=1$ and $\nu=-1$ first and then enters the trivial phase $\nu=0$ with variation of the parameter $\theta\in[0,\pi]$. The phase transition usually means the closing of the gap, which indicates that the topological excitation transmission experiences two gap closing points within $\theta_t\in[0,\pi]$. In contrast, if we introduce the phase factor $\gamma$ now, the nonvanishing phase factor can destroy the topological phase with $\nu=-1$, as shown in Fig. 5(d). For example, when $\gamma=-\pi$ and $|J|=1$, we find that the system only experiences

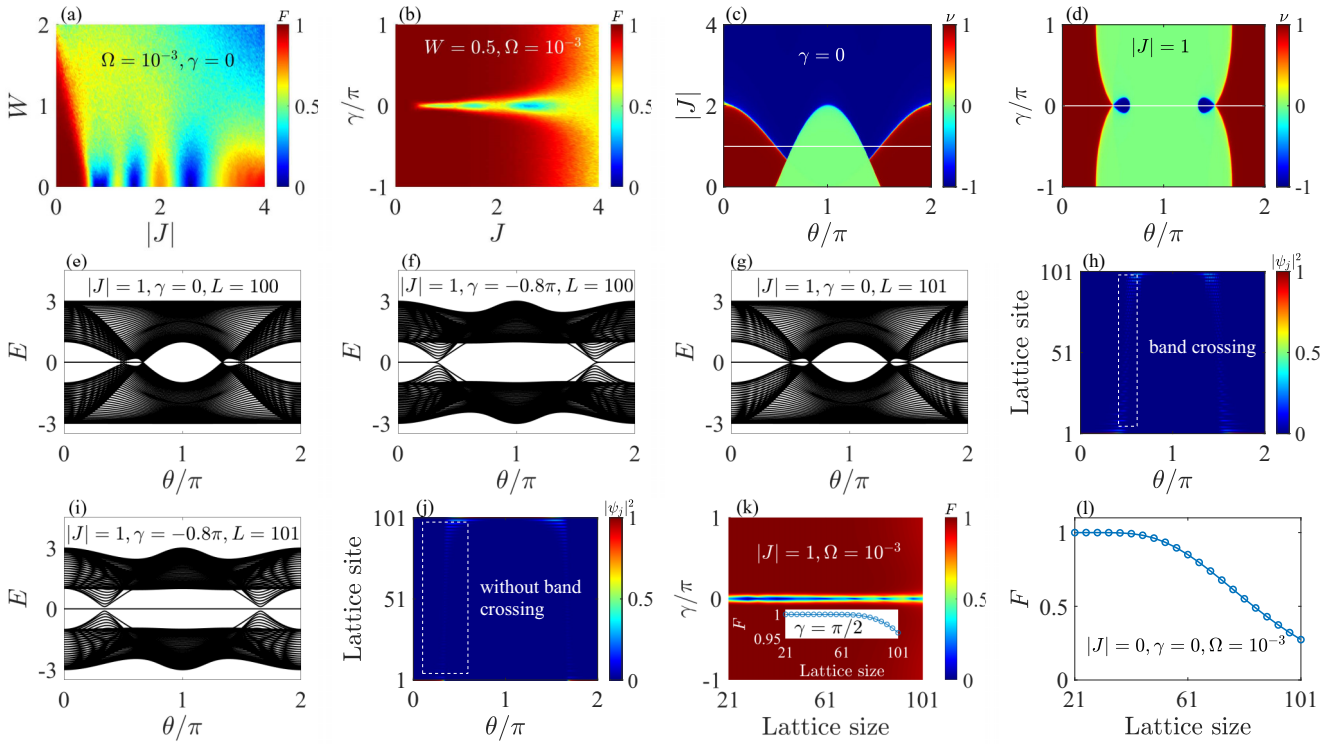


FIG. 5. Robustness, phase diagrams, energy spectra, and distributions of states when when $r = 2$ and $l = 1$. (a) Fidelity versus hopping amplitude $|J|$ and disorder strength $W$ when $L = 21$. (b) Fidelity versus hopping amplitude $|J|$ and phase factor $\gamma$ when $W = 0.5$ and $L = 21$. (c) Phase diagram versus the parameters $\theta$ and $|J|$ when $L = 300$. The white line represents $|J| = 1$. (d) Phase diagram versus the parameters $\theta$ and $\gamma$ when $|J| = 1$ and $L = 300$. The white line represents $\gamma = 0$. (e) Energy spectra when $|J| = 1$, $\gamma = 0$, and $L = 100$. (f) Energy spectra when $|J| = 1$, $\gamma = -0.8\pi$, and $L = 100$. (g) Energy spectrum and (h) distribution of the zero-energy mode when $|J| = 1$, $\gamma = 0$, and $L = 101$. (i) Energy spectrum and (j) distribution of the zero-energy mode when $|J| = 1$, $\gamma = -0.8\pi$, and $L = 101$. (k) Fidelity versus phase factor and lattice size when $|J| = 1$ and $\Omega = 10^{-3}$. (l) Fidelity versus lattice size when $|J| = 0$, $\gamma = 0$, and $\Omega = 10^{-3}$.

one phase transition from $\nu = 1$ to $\nu = 0$ within $\theta \in [0, \pi]$, meaning that one of the two original gap closing points may be reopened.

Note that the phase diagram can also be obtained by defining the winding number in momentum space since the boundary effect cannot affect the bulk topology (see Appendix A). Thus, the possible reopening of the gap mentioned above can be estimated analytically via the Hamiltonian in momentum. The Hamiltonian in Eq. (1) in the momentum space can be written as

$$h(k) = h_x\sigma_x + h_y\sigma_y, \tag{5}$$

where $\sigma_j$ $(j = x, y)$ is the Pauli matrix and $h_x = J_1 + J_2\cos k + |J|\cos(\gamma + k)$ and $h_y = J_2\sin k - |J|\sin(\gamma + k)$ are the corresponding amplitudes. Obviously, the gap of the system is closed when $\Delta = 2\sqrt{h_x^2 + h_y^2} = 0$, at which point the system may experience the phase transition. As shown in Fig. 5(c), when $|J| = 1$ and $\gamma = 0$, the system experiences two phase transitions within $\theta \in [0, \pi]$, while a certain value of the phase factor $\gamma$ can eliminate the topological phase with $\nu = -1$ [see Fig. 5(d)]. The vanishing of the topological phase with $\nu = -1$ means that the corresponding gap closing point may be reopened by the phase factor $\gamma$. In the following, we take $\gamma = 0$ and $\gamma \neq 0$ as two examples to clarify the vanishing of the gap closing point. When $k = \pi$, we have $h_x = J_1 - J_2 - |J|\cos\gamma$ and $h_y = |J|\sin\gamma$, meaning that the corresponding gap satisfies $\Delta = 2\sqrt{4\cos^2\theta + 4|J|\cos\gamma\cos\theta + |J|^2}$. Obviously, when $\gamma = 0$, the gap is closed under the parameter regime of

$$\cos\theta = -\frac{|J|}{2}, \tag{6}$$

which just corresponds to the phase transition point between the nontrivial phase with $\nu = -1$ and the trivial phase with $\nu = 0$ ($\theta = 2/3\pi$ and $4/3\pi$). In contrast, if $\gamma \neq 0$, we have $\Delta \neq 0$ for the same condition of $\cos\theta = -|J|/2$, implying that the gap closing point now may be opened by the phase factor $\gamma$. In this way, the phase factor $\gamma$ can decrease the number of gap closing points for a certain $|J|$, which further promotes the topological excitation transmission.

To further verify the above analysis, we plot the energy spectra for different $|J|$ and $\gamma$ when $L = 100$ in Figs. 5(e) and 5(f). The energy spectra agree well with the phase diagrams and clearly show the decreasing of gap closing points induced by nonzero $\gamma$. The decreasing of gap closing points naturally can affect the topological channel of excitation transmission, as shown in Figs. 5(g)–5(j). More specifically, the zero-energy mode (topological channel) experiences two gap closing points around $\theta \sim 0.5\pi$ [Fig. 5(g)] when $\gamma = 0$ and $|J| = 1$, which leads to the zero-energy mode being able to enter the bulk (generating band crossing and bulk diffusion) around $\theta \sim 0.5\pi$ in the evolution process [Fig. 5(h)]. In this way, the topological excitation transmission may be invalid

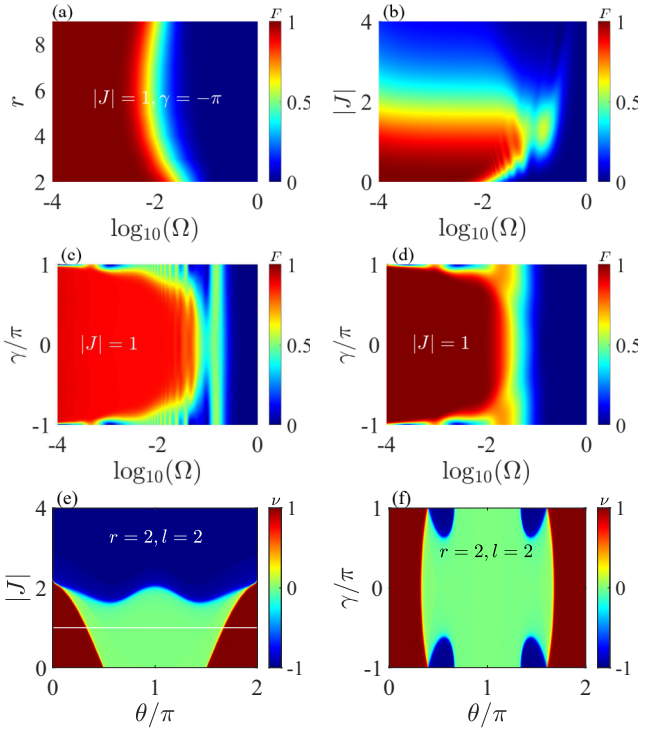


FIG. 6. Extended cases for topological excitation transmission assisted by the phase factor. (a) Fidelity versus evolution speed $\Omega$ and the structure parameter $r$ when $l = 1$, $|J| = 1$, and $\gamma = -\pi$. (b) Fidelity versus evolution speed $\Omega$ and the parameter $|J|$ when $r = 1$, $l = 2$, and $\gamma = 0$. (c) Fidelity versus evolution speed $\Omega$ and phase $\gamma$ when $r = 1$, $l = 2$, and $|J| = 1$. (d) Fidelity versus evolution speed $\Omega$ and phase $\gamma$ when $r = 2$, $l = 2$, and $|J| = 1$. (e) Phase diagram versus the parameters $\theta$ and $|J|$ when $r = 2$, $l = 2$, and $\gamma = 0$. The white line denotes $|J| = 1$. (f) Phase diagram versus the parameters $\theta$ and $\gamma$ when $r = 2$, $l = 2$, and $|J| = 1$.

due to the bulk diffusion. However, when $\gamma = -0.8\pi$ and $|J| = 1$, the gap closing point becomes once again around $\theta \sim 0.5\pi$ [Fig. 5(i)] and the system corresponds to a large minimal energy space $\Delta_E$. The decreasing of the gap closing point and enlarged $\Delta_E$ ensures the transmission efficiency and robustness. Furthermore, we also investigate the finite-size effects on the phase-factor-optimized topological transmission and find that the phase-factor-optimized topological transmission is much more robust to the finite-size effect [Fig. 5(k)] compared with the topological transmission in the standard SSH model [Fig. 5(l)].

### D. Generalization and discussion

Before concluding, we further discuss the cases of $r \geqslant 2$ or $l > 1$. We first focus on the case of $r \geqslant 2$ and $l = 1$. In Fig. 6(a) we plot the transmission fidelity versus the parameter $r$ and evolution speed $\Omega$. We find that the enlarged $r$ will weaken the transmission efficiency first and enhance the transmission again. The transmission fidelity when $r = 1$ and $l = 2$ (longer-range hopping) is shown in Fig. 6(b), which reveals that a certain hopping amplitude $|J|$ in longer-range hopping can weaken the transmission and a large enough amplitude $|J|$ can even destroy the transmission. For example, when $|J| = 1$, we find that the excitation cannot be transmitted to the right edge completely and the large phase factor $\gamma$ (e.g., $\gamma = \pm\pi$) now can inhibit the topological transmission, as shown in Fig. 6(c). To improve the transmission fidelity, we still can perform a similar operation via removing the hopping between sites $a_1$ and $b_3$, i.e., $r = 2$. The fidelity versus the phase factor $\gamma$ and evolution speed when $r = 2$ and $l = 2$ is plotted in Fig. 6(d), which shows that the excitation can be transmitted to the right edge completely only when the phase factor $\gamma$ is not around $\gamma = \pm\pi$.

The reason why the large phase factor cannot promote the transmission when $l = 2$ can still be explained by the phase transition, as shown in Figs. 6(e) and 6(f). We find that, when $r = 2$, $l = 2$, and $|J| = 1$, the system experiences only one phase transition within $\theta \in [0, \pi]$ [see white line in Fig. 6(e)], which is different from the case shown in Fig. 5(c). In particular, the small phase factor $\gamma$ also cannot induce a new phase transition [see Fig. 6(e)], making the optimized transmission scheme induced by the phase factor invalid. However, when the phase factor $\gamma$ is large enough, e.g., $\gamma = \pm\pi$, the large enough phase factor now can induce a new phase transition, meaning that the system experiences two closing gap points when $\gamma = \pm\pi$. In this way, the large phase factor $\gamma$ will inhibit the topological excitation transmission. Thus, when we implement the phase-factor-optimized topological excitation transmission, we need to make a reasonable choice of the order of long-range hopping, i.e., the value of the parameter $l$.

We stress that all of the conclusions on the phase-factor-optimized topological excitation transmission are obtained when the long-range hopping is added between sites of $b_{n+l}$ and $a_n$, which may become different when the long-range hopping has different forms, e.g., the long-range hopping is added between two sites of the same type or between sites of $a_{n+l}$ and $b_n$ (see Appendix B). Furthermore, we also stress that the phase-factor-optimized topological transmission scheme may not be suitable to an arbitrary one-dimensional lattice, e.g., the Kitaev model (see Appendix C).

## III. CONCLUSION

We have shown the effects of the phase factor in long-range hopping on the topological excitation transmission. We found that the phase factor can enhance the topological excitation transmission weakened by the finite amplitude of long-range hopping. This enhanced topological transmission can be comprehended by the widened minimal energy space around the gap closing point, which reveals the important effects of the phase factor on the topological excitation transmission. Furthermore, we showed the perfect topological excitation transmission enhanced by the phase factor of long-range hopping by optimizing the configuration of long-range hopping. In particular, we found that the enhanced topological transmission originates from the decreasing of the gap closing point induced by the phase factor, which confirms the non-negligible role of the phase factor in the phase transition. Our investigation has revealed the effects of the phase factor in long-range hopping on the topological excitation transmission, which may provide different perspectives on the importance of the phase factor in terms of the hopping strength.

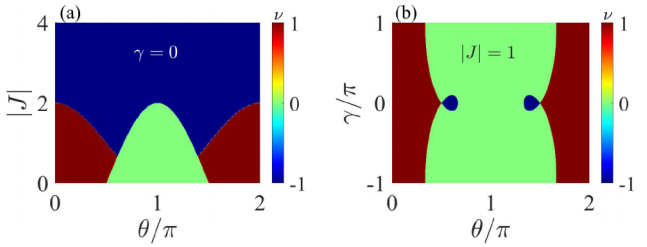


FIG. 7. Phase diagrams in momentum space. (a) Phase diagram in momentum space versus the parameters $\theta$ and $|J|$ when $l = 2$ and $\gamma = 0$. The white line denotes $|J| = 1$. (b) Phase diagram in momentum space versus the parameters $\theta$ and $\gamma$ when $l = 2$ and $|J| = 1$.


## ACKNOWLEDGMENT

This work was supported by the National Natural Science Foundation of China (Grants No. 12304557 and No. 12204404) and China Postdoctoral Science Foundation (Grant No. 2024M752757).


## APPENDIX A: PHASE DIAGRAMS IN MOMENTUM SPACE

In Figs. 5(c) and 5(d) we show the phase diagrams in real space since the lack of long-range hopping between sites $a_1$ and $b_2$ destroys the translational symmetry of the lattice. We stress that when the size of the lattice is large enough, the boundary effect induced by the lack of long-range hopping between sites $a_1$ and $b_2$ can be regarded as a perturbation compared with bulk, resulting in the phase diagram defined by the winding number in real space having the same pattern as the phase diagram defined by the winding number in momentum space. In Fig. 7 we plot the phase diagrams defined by the winding number in momentum space, i.e., $\nu = \frac{1}{2\pi}\int_{-\pi}^{\pi} \frac{h_x\partial_k h_y - h_y\partial_k h_x}{h_x^2+h_y^2}dk$. Here $h_x = J_1 + J_2\cos k + |J|\cos(\gamma + k)$ and $h_y = J_2\sin k - |J|\sin(\gamma + k)$ are the corresponding components after rewriting the Hamiltonian in momentum space as $h(k) = h_x\sigma_x + h_y\sigma_y$. The results clearly show the same phase diagrams compared as in Figs. 5(c) and 5(d), meaning that we can also estimate the bulk topology via the winding number in momentum space. In this way, we can calculate the variation of the gap closing point (phase transition point) analytically via the Hamiltonian in momentum space.

## APPENDIX B: DIFFERENT FORMS OF LONG-RANGE HOPPING

We have shown that the phase factor can optimize the topological transmission when the long-range hopping is added between sites of $b_{n+l}$ and $a_n$, which may become different when the forms of long-range hopping are different. For example, we now consider a SSH model with multifold long-range hopping, i.e.,

$$H = \sum_n [J_1 a_n^\dagger b_n + J_2 a_{n+1}^\dagger b_n + |J_3| e^{i\phi}(a_{n+l}^\dagger a_n + b_{n+l}^\dagger b_n) + |J_4| e^{i\gamma}(b_{n+l}^\dagger a_n + a_{n+l}^\dagger b_n)] + \text{H.c.} \quad \text{(B1)}$$

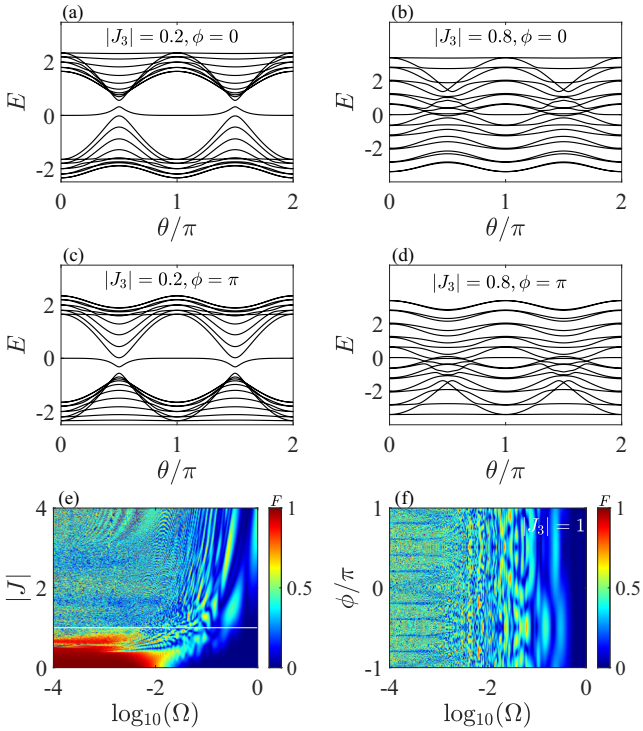


FIG. 8. Energy spectra and fidelities when $|J_3| \neq 0$ and $|J_4| = 0$. The energy spectra are shown for (a) $|J_3| = 0.2$ and (b) $|J_3| = 0.8$ when $\phi = 0$ and $l = 2$ and (c) $|J_3| = 0.2$ and (d) $|J_3| = 0.8$ when $\phi = \pi$ and $l = 2$. (e) Transmission fidelity versus the parameter $|J_3|$ and varying speed when $\phi = 0$. The white line denotes $|J_3| = 1$. (f) Transmission fidelity versus the parameter $\phi$ and varying speed when $|J_3| = 1$. The size of the lattice is $L = 21$.

In the momentum space, the above Hamiltonian can be rewritten as

$$h(k) = h_0 I + h_x\sigma_x + h_y\sigma_y, \quad \text{(B2)}$$

where $I$ is the unit matrix and $h_0 = 2|J_3|\cos(\phi + kl)$, $h_x = J_1 + J_2\cos k + 2|J_4|\cos(\gamma - kl)$, and $h_y = J_2\sin k$ are the corresponding amplitudes. Note that the existence of the term $h_0 I$ only moves the energy bands and cannot change the corresponding eigenstates, implying that the above Hamiltonian $h(k)$ has the same bulk topology with the Hamiltonian $h'(k) = h_x\sigma_x + h_y\sigma_y$, i.e., the existence of the long-range hopping of $|J_3|e^{i\phi}(a_{n+l}^\dagger a_n + b_{n+l}^\dagger b_n)$ cannot affect the phase transition. We stress that, although the long-range hopping between the same type of sites cannot induce the phase transition, it can deform the corresponding energy spectrum. For example, Figs. 8(a)–8(d) show the energy spectra for different $|J_3|$ and $\phi$ when $|J_4| = 0$. Obviously, both the parameters $|J_3|$ and $\phi$ can affect the energy spectrum, implying that they may have effects on the topological transmission. To further explore the possible effects of long-range hopping between the same type of sites on topological transmission, we plot the corresponding transmission fidelities, as shown in Figs. 8(e) and 8(f). The results reveal that although the parameter $|J|$ can affect the transmission, the phase factor $\phi$ cannot optimize the affected transmission. It can be easily understood by the fact that

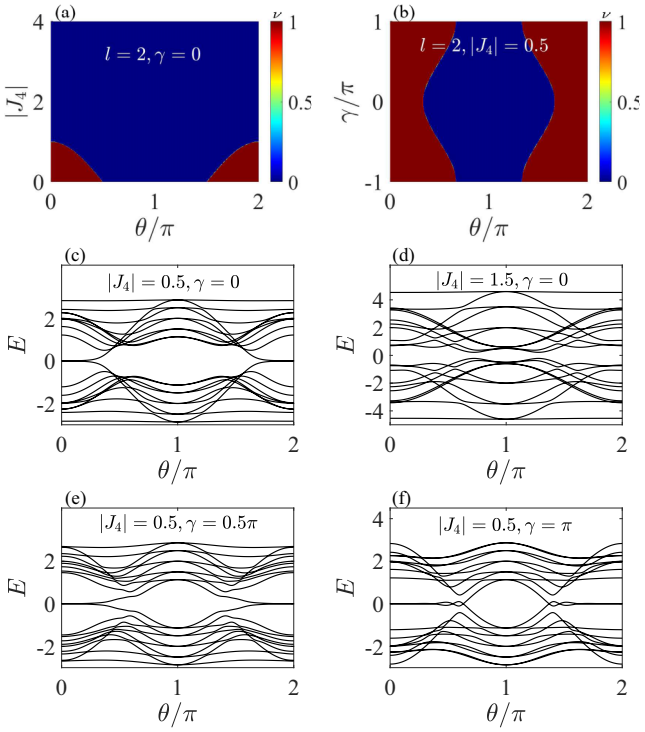


FIG. 9. Phase diagrams and energy spectra when $|J_3| = 0$ and $|J_4| \neq 0$. (a) Phase diagram in momentum space versus the parameters $\theta$ and $|J|$ when $l = 2$ and $\gamma = 0$. (b) Phase diagram in momentum space versus the parameters $\theta$ and $\gamma$ when $l = 2$ and $|J_4| = 0.5$. Also shown are the energy spectra for (c) $|J_4| = 0.5$ and $\gamma = 0$, (d) $|J_4| = 1.5$ and $\gamma = 0$, (e) $|J_4| = 0.5$ and $\gamma = 0.5\pi$, and (f) $|J_4| = 0.5$ and $\gamma = \pi$ when $L = 20$.

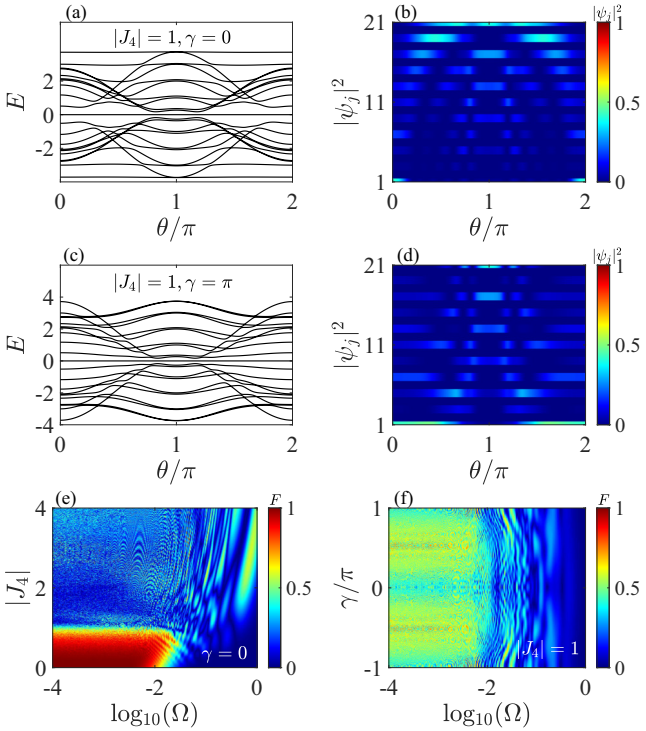


FIG. 10. Energy spectra, distributions of the gap state, and fidelities when $|J_3| = 0$ and $|J_4| \neq 0$. (a) Energy spectra and (b) distribution of the gap state when $|J_4| = 1$, $\gamma = 0$, and $l = 2$. (c) Energy spectra and (d) distribution of the gap state when $|J_4| = 1$, $\gamma = \pi$, and $l = 2$. (e) Transmission fidelity versus the parameter $|J_4|$ and varying speed when $\gamma = 0$ and $l = 2$. (f) Transmission fidelity versus the parameter $\gamma$ and varying speed when $|J_3| = 1$ and $l = 2$. The size of the lattice is $L = 21$.

neither of the parameters $|J|$ and $\phi$ can induce a new phase transition.

Now we focus on the case of $|J_3| = 0$ and $|J_4| \neq 0$. We consider first the possible phase transition induced by the parameters $|J_4|$ and $\gamma$. The corresponding phase diagrams are plotted in Figs. 9(a) and 9(b). The results indicate that the parameters $|J_4|$ and $\gamma$ can only change the range of the nontrivial phase but cannot induce a new topological phase transition, which is different from the cases shown in Figs. 5(c) and 5(d). To further verify the above analysis, we also plot the energy spectra for different $|J_4|$ and $\gamma$ in Figs. 9(c)–9(f). Obviously, the energy spectra agree well with the phase diagram. To further investigate the effects of $|J_4|$ and $\gamma$ on the topological transmission, we plot in Fig. 10 the energy spectra, distributions of the zero-energy mode, and transmission fidelities for different $|J_4|$ and $\gamma$ when the lattice size is an odd number. The results reveal that the large amplitude of long-range hopping can totally destroy the topological channel of excitation transmission, as shown in Figs. 10(a) and 10(b). Meanwhile, the nonzero phase factor $\gamma$ in the long-range hopping now cannot optimize the destroyed topological channel [Figs. 10(c) and 10(d)], implying that the phase-factor-optimized transmission scheme may not be implemented in such a model. The results of fidelities [Figs. 10(e) and 10(f)] further verify the above inference, in which the phase factor $\gamma$ now cannot optimize the transmission efficiency for the finite parameter $|J_4|$. Thus, to implement the robust topological transmission optimized by the phase factor of long-range hopping, the form of long-rang hopping needs to be well designed.

## APPENDIX C: APPLICABILITY TO THE KITAEV MODEL

Note that, according to the equivalence between the SSH model and Kitaev model, the Kitaev model with the long-range hopping may implement similar phase-factor-optimized topological transmission. Actually, we can prove that the Kitaev model with long-range hopping is equivalent to the model shown in Eq. (B1), implying that the long-range hopping in the Kitaev model cannot implement the phase-factor-optimized transmission scheme. For example, for the Kitaev model with long-range hopping, i.e.,

$$H = \sum_j \mu c_j^\dagger c_j + \sum_j [t(c_{j+1}^\dagger c_j + c_{j+1}^\dagger c_j^\dagger + \text{H.c.}) + |J| e^{i\gamma} c_{j+l}^\dagger c_j + |J| e^{-i\gamma} c_j^\dagger c_{j+l}], \tag{C1}$$

it can be rewritten based on the Majorana basis, with

$$H = \frac{1}{4} \sum_j [i\mu \xi_{1,j} \xi_{2,j} + 2it \xi_{1,j} \xi_{2,j+1} + i|J| \sin\gamma (\xi_{1,j+l} \xi_{1,j} + \xi_{2,j+l} \xi_{2,j}) + i|J| \cos\gamma (\xi_{1,j+l} \xi_{2,j} + \xi_{1,j} \xi_{2,j+l})] + \text{H.c.}, \tag{C2}$$

where $\xi_{1,j} = c_j + c_j^\dagger$ and $\xi_{2,j} = i(c_j^\dagger - c_j)$ are the Majorana operators. Obviously, the above Hamiltonian is equivalent to a SSH chain with long-range hopping after replacing the symbols $\xi_{1,j}$ and $\xi_{2,j}$ with $b_n$ and $a_n$, i.e.,

$$H = \frac{1}{4}\sum_n [-i\mu a_n^\dagger b_n + 2it a_{n+1}^\dagger b_n + i|J|\sin\gamma(a_{n+l}^\dagger a_n + b_{n+l}^\dagger b_n) + i|J|\cos\gamma(b_{n+l}^\dagger a_n - a_{n+l}^\dagger b_n)] + \text{H.c.} \tag{C3}$$

The Hamiltonian in Eq. (C3) obviously has the same form as Eq. (B1), indicating that the phase-factor-optimized topological transmission cannot be implemented in the Kitaev model with long-range hopping.


[1] D. J. Thouless, Quantization of particle transport, Phys. Rev. B **27**, 6083 (1983).

[2] S. Nakajima, T. Tomita, S. Taie, T. Ichinose, H. Ozawa, L. Wang, M. Troyer, and Y. Takahashi, Topological Thouless pumping of ultracold fermions, Nat. Phys. **12**, 296 (2016).

[3] Y. Ke, X. Qin, Y. S. Kivshar, and C. Lee, Multiparticle Wannier states and Thouless pumping of interacting bosons, Phys. Rev. A **95**, 063630 (2017).

[4] L. Lin, Y. Ke, and C. Lee, Interaction-induced topological bound states and Thouless pumping in a one-dimensional optical lattice, Phys. Rev. A **101**, 023620 (2020).

[5] S. Hu, Y. Ke, and C. Lee, Topological quantum transport and spatial entanglement distribution via a disordered bulk channel, Phys. Rev. A **101**, 052323 (2020).

[6] M. Jürgensen, S. Mukherjee, and M. C. Rechtsman, Quantized nonlinear Thouless pumping, Nature (London) **596**, 63 (2021).

[7] R. Citro and M. Aidelsburger, Thouless pumping and topology, Nat. Rev. Phys. **5**, 87 (2023).

[8] Y. E. Kraus, Y. Lahini, Z. Ringel, M. Verbin, and O. Zilberberg, Topological states and adiabatic pumping in quasicrystals, Phys. Rev. Lett. **109**, 106402 (2012).

[9] M. Verbin, O. Zilberberg, Y. Lahini, Y. E. Kraus, and Y. Silberberg, Topological pumping over a photonic Fibonacci quasicrystal, Phys. Rev. B **91**, 064201 (2015).

[10] M. Bello, C. Creffield, and G. Platero, Long-range doublon transfer in a dimer chain induced by topology and ac fields, Sci. Rep. **6**, 22562 (2016).

[11] C. Dlaska, B. Vermersch, and P. Zoller, Robust quantum state transfer via topologically protected edge channels in dipolar arrays, Quantum Sci. Technol. **2**, 015001 (2017).

[12] N. Lang and H. P. Büchler, Topological networks for quantum communication between distant qubits, npj Quantum Inf. **3**, 47 (2017).

[13] M. P. Estarellas, I. D'Amico, and T. P. Spiller, Topologically protected localised states in spin chains, Sci. Rep. **7**, 42904 (2017).

[14] J. L. Tambasco, G. Corrielli, R. J. Chapman, A. Crespi, O. Zilberberg, R. Osellame, and A. Peruzzo, Quantum interference of topological states of light, Sci. Adv. **4**, eaat3187 (2018).

[15] F. Mei, G. Chen, L. Tian, S.-L. Zhu, and S. Jia, Robust quantum state transfer via topological edge states in superconducting qubit chains, Phys. Rev. A **98**, 012331 (2018).

[16] M. I. N. Rosa, R. K. Pal, J. R. F. Arruda, and M. Ruzzene, Edge states and topological pumping in spatially modulated elastic lattices, Phys. Rev. Lett. **123**, 034301 (2019).

[17] S. Longhi, G. L. Giorgi, and R. Zambrini, Landau–Zener topological quantum state transfer, Adv. Quantum Technol. **2**, 1800090 (2019).

[18] S. Longhi, Topological pumping of edge states via adiabatic passage, Phys. Rev. B **99**, 155150 (2019).

[19] L. Qi, G. L. Wang, S. Liu, S. Zhang, and H.-F. Wang, Controllable photonic and phononic topological state transfers in a small optomechanical lattice, Opt. Lett. **45**, 2018 (2020).

[20] F. M. D'Angelis, F. A. Pinheiro, D. Guéry-Odelin, S. Longhi, and F. Impens, Fast and robust quantum state transfer in a topological Su-Schrieffer-Heeger chain with next-to-nearest-neighbor interactions, Phys. Rev. Res. **2**, 033475 (2020).

[21] P. Gao and J. Christensen, Topological sound pumping of zero-dimensional bound states, Adv. Quantum Technol. **3**, 2000065 (2020).

[22] N. E. Palaiodimopoulos, I. Brouzos, F. K. Diakonos, and G. Theocharis, Fast and robust quantum state transfer via a topological chain, Phys. Rev. A **103**, 052409 (2021).

[23] Y. X. Shen, L. S. Zeng, Z. G. Geng, D. G. Zhao, Y. G. Peng, and X. F. Zhu, Acoustic adiabatic propagation based on topological pumping in a coupled multicavity chain lattice, Phys. Rev. Appl. **14**, 014043 (2020).

[24] J. X. Han, J. L. Wu, Y. Wang, Y. Xia, Y. Y. Jiang, and J. Song, Large-scale Greenberger-Horne-Zeilinger states through a topologically protected zero-energy mode in a superconducting qutrit-resonator chain, Phys. Rev. A **103**, 032402 (2021).

[25] J. N. Zhang, J. L. Wu, J. X. Han, S. Tang, J. Song, and Y. Y. Jiang, Small admixture of nonadiabaticity facilitating topologically protected splitters and routers via optimizing coupling engineering, Phys. Rev. B **109**, 094303 (2024).

[26] M. Z. Hasan and C. L. Kane, Colloquium: Topological insulators, Rev. Mod. Phys. **82**, 3045 (2010).

[27] X. L. Qi and S. C. Zhang, Topological insulators and superconductors, Rev. Mod. Phys. **83**, 1057 (2011).

[28] C. K. Chiu, J. C. Y. Teo, A. P. Schnyder, and S. Ryu, Classification of topological quantum matter with symmetries, Rev. Mod. Phys. **88**, 035005 (2016).

[29] A. Bansil, H. Lin, and T. Das, Colloquium: Topological band theory, Rev. Mod. Phys. **88**, 021004 (2016).

[30] F. D. M. Haldane, Model for a quantum Hall effect without Landau levels: Condensed-matter realization of the "parity anomaly", Phys. Rev. Lett. **61**, 2015 (1988).

[31] D. Sticlet and F. Piéchon, Distant-neighbor hopping in graphene and Haldane models, Phys. Rev. B **87**, 115402 (2013).

[32] A. Rüegg, J. Wen, and G. A. Fiete, Topological insulators on the decorated honeycomb lattice, Phys. Rev. B **81**, 205115 (2010).

[33] X. Hu, M. Kargarian, and G. A. Fiete, Topological insulators and fractional quantum Hall effect on the ruby lattice, Phys. Rev. B **84**, 155116 (2011).

[34] J. H. Jiang, Tunable topological Weyl semimetal from simple-cubic lattices with staggered fluxes, Phys. Rev. A **85**, 033640 (2012).

[35] A. L. He, L. R. Ding, Y. Zhou, Y. F. Wang, and C. D. Gong, Quasicrystalline Chern insulators, Phys. Rev. B **100**, 214109 (2019).

[36] Y. Han, Y. Zhou, and A. L. He, $C_n$-symmetric quasi-periodic Chern insulators, New J. Phys. **26**, 033003 (2024).

[37] M. Kargarian and G. A. Fiete, Topological phases and phase transitions on the square-octagon lattice, Phys. Rev. B **82**, 085106 (2010).

[38] K. Sun, Z. Gu, H. Katsura, and S. Das Sarma, Nearly flatbands with nontrivial topology, Phys. Rev. Lett. **106**, 236803 (2011).

[39] R. Liu, W. C. Chen, Y. F. Wang, and C. D. Gong, Topological quantum phase transitions and topological flat bands on the kagomé lattice, J. Phys.: Condens. Matter **24**, 305602 (2012).

[40] W. C. Chen, R. Liu, Y. F. Wang, and C. D. Gong, Topological quantum phase transitions and topological flat bands on the star lattice, Phys. Rev. B **86**, 085311 (2012).

[41] X. P. Liu, W. C. Chen, Y. F. Wang, and C. D. Gong, Topological quantum phase transitions on the kagomé and square–octagon lattices, J. Phys.: Condens. Matter **25**, 305602 (2013).

[42] Z. Y. Lan, A. L. He, and Y. F. Wang, Flat bands with high Chern numbers and multiple flat bands in multifold staggered-flux models, Phys. Rev. B **107**, 235116 (2023).

[43] Y. Otaki and T. Fukui, Higher-order topological insulators in a magnetic field, Phys. Rev. B **100**, 245108 (2019).

[44] Z. R. Liu, C. B. Hua, T. Peng, R. Chen, and B. Zhou, Higher-order topological insulators in hyperbolic lattices, Phys. Rev. B **107**, 125302 (2023).

[45] B. Wang, X. Zhou, H. Lin, and A. Bansil, Higher-order topological insulator phase in a modified Haldane model, Phys. Rev. B **104**, L121108 (2021).

[46] A. L. He, W. W. Luo, Y. Zhou, Y. F. Wang, and H. Yao, Topological states in a dimerized system with staggered magnetic fluxes, Phys. Rev. B **105**, 235139 (2022).

[47] A. L. He, X. Zhang, and Y. Liu, Topological states in a dimerized square-octagon lattice with staggered magnetic fluxes, Phys. Rev. B **106**, 125147 (2022).

[48] D. H. Guan, L. Qi, X. Zhang, Y. Liu, and A. L. He, Staggered magnetic flux induced higher-order topological insulators and topological flat bands on the ruby lattice, Phys. Rev. B **108**, 085121 (2023).

[49] A. L. He, X. H. Yan, L. Qi, Y. Liu, and Y. Han, Topological states and flat bands on the maple leaf lattice, Phys. Rev. B **109**, 075118 (2024).

[50] I. Mondragon-Shem, T. L. Hughes, J. Song, and E. Prodan, Topological criticality in the chiral-symmetric AIII class at strong disorder, Phys. Rev. Lett. **113**, 046802 (2014).

[51] J. Song and E. Prodan, AIII and BDI topological systems at strong disorder, Phys. Rev. B **89**, 224203 (2014).

[52] D. W. Zhang, L. Z. Tang, L. J. Lang, H. Yan, and S. L. Zhu, Non-Hermitian topological anderson insulators, Sci. China Phys. Mech. Astron. **63**, 267062 (2020).

[53] L. Lin, Y. Ke, and C. Lee, Real-space representation of the winding number for a one-dimensional chiral-symmetric topological insulator, Phys. Rev. B **103**, 224208 (2021).